

COMPUTATIONAL MODELING, ONTOGENY, AND BIOMECHANICS OF
CRANIAL FORCES IN *ALLIGATOR MISSISSIPPIENSIS*

A Thesis
presented to
the Faculty of the Graduate School
at the University of Missouri-Columbia

In Partial Fulfillment
of the Requirements for the Degree
Master of Science

by

KALEB CRAIG SELLERS

Dr. Casey M. Holliday, Thesis Supervisor

JULY 2015

The undersigned, appointed by the dean of the Graduate School, have examined the thesis entitled

COMPUTATIONAL MODELING, ONTOGENY, AND BIOMECHANICS OF
CRANIAL FORCES IN *ALLIGATOR MISSISSIPPIENSIS*

presented by Kaleb Craig Sellers,

a candidate for the degree of master of sciences, and hereby certify that, in their opinion, it is worthy of acceptance.

Professor Casey M. Holliday

Professor Kevin Middleton

Professor Libby Cowgill

ACKNOWLEDGEMENTS

Thanks to Dr. Casey Holliday, Dr. Kevin Middleton, and Dr. Libby Cowgill for sitting on my committee and providing superb advice. Thanks to the Missouri Research Board and the Missouri Research Council for funding. Thanks to the Department of Pathology and Integrative Anatomy at the University of Missouri for help and support of every type. Thanks Ruth Elsey at Rockefeller Wildlife Refuge for providing specimens, and to the School of Medicine and the School of Veterinary Medicine at the University of Missouri for scanning specimens. Thanks to Dr. Julian Davis for assistance with FEA software and answering numerous math questions.

TABLE OF CONTENTS

ACKNOWLEDGEMENTS	ii
LIST OF FIGURES	iv
LIST OF TABLES	v
Chapter	
1. INTRODUCTION	1
2. MATERIALS AND METHODS	7
Specimens and Model Construction	
Myology	
Joints	
3D Lever Analysis	
Finite Element Analysis	
Comparison of Calculated Forces with <i>In Vivo</i> Data	
3. RESULTS	13
Muscles and Models	
Bite Force	
Joint Forces	
Statistical Analyses	
4. DISCUSSION	17
Effects of Gape and Bite Position	
Comparison of Bite Forces with <i>In Vivo</i> Data	
Joint Forces	
Application to Extinct Taxa	
5. CONCLUSIONS	23

FIGURES	24
TABLES	31
LITERATURE CITED	44

LIST OF FIGURES

Figure	Page
1. Skull of <i>Alligator mississippiensis</i>	24
2. Joints in study	25
3. Process of model generation	26
4. Muscle maps.....	27
5. Joint axes	28
6. Calculation of moments about axis	29
7. Change in bite force orientation and magnitude with bite position	30

LIST OF TABLES

Table	Page
1. Jaw muscle forces.....	31
2. Contribution of muscles to total muscle force.....	32
3. Moments about jaw joint axis	33
4. Contribution of each muscle to bite force	34
5. Bite force calculated with lever mechanics and finite element analysis	35
6. Jaw joint forces.....	36
7. Pterygomandibular joint forces	37
8. Components of bite force and jaw joint force for posterior bite	38
9. Components of bite force and jaw joint force for intermediate bite	39
10. Components of bite force and jaw joint force for anterior bite	40
11. Reduced major axis regression analysis of forces for posterior bite.....	41
12. Reduced major axis regression analysis of forces for intermediate bite	42
13. Reduced major axis regression analysis of forces for anterior bite.....	43

INTRODUCTION

Bite force performance is linked to a variety of dietary adaptations among vertebrates. Recent studies have shown that bite force, cranial morphology, and dietary ecology are correlated in finches (Herrel et al. 2005), crocodylians (Erickson et al. 2003; Gignac and Erickson 2015), canids (Slater et al. 2009) and phyllostomid bats (Dumont et al. 2004; Santana 2011), among others. High relative bite force can permit the exploitation of a wider range of food. Darwin's finches represent a classic case of adaptive radiation via ecomorphological differentiation. It has been shown that finches with higher bite forces are capable of exploiting larger, more robust seeds and nuts (Herrel et al. 2005). Beak morphology corresponds with bite force; finches that deliver more powerful bites have wider beaks relative to body size (Herrel et al. 2005). Hard biting dogs have crania optimized for dissipating cranial forces and specialize in hunting larger vertebrates compared to those with lower maximum bite forces and generalist diets (Slater et al. 2009). Similarly, phyllostomid bats with high bite force performance relative to closely related taxa consume a wider variety of foods (Santana et al. 2011). Finally, in the American alligator, ontogenetic shifts in dietary niche have been attributed in part to increasing bite force (Busbey 1989; Erickson et al. 2003; Gignac and Erickson 2015). As individuals produce forces capable of fracturing harder food, they add more robust prey items to the diet. Hatchlings take primarily insects, and add crustaceans, fish, amphibians and small reptiles at a young age. Mid-sized individuals eat primarily smaller mammals

and birds, whereas mature animals take large fish, large birds, turtles, and large mammals.

Understanding the production of forces during feeding and the manner in which the skull resists reaction forces can offer insights into the evolution of skull function. Biting produces forces at craniomandibular joints and teeth. In gnathostomes, contraction of the jaw adductor muscles rotates the mandible. If a food item is held in the mouth, the food will be moved by the mandibular rotation until the upper jaws resist further adduction. At this point, the force that was previously moving the food item is met with a reaction force from the upper jaw, bringing the system into static equilibrium. Applied forces may increase until the food item yields such as in crushing.

When a skull applies force to an object during biting, Newton's third law dictates that a reaction force is also applied to the skull. Reaction forces act on the mandible both at the point of contact with the food item and at any points of contact between the cranium and mandible that resist the action of the adductor muscles, such as the jaw joint. The magnitude and direction of reaction forces depend on factors such as gape (Dumont and Herrel 2003) the position of the bite along the tooth row (Bramble 1978; Sinclair and Alexander 1987; Dumont and Herrel 2003), and magnitude and geometry of muscular (input) forces. The morphology of the jaw joint has been suggested to reflect the orientation of reaction forces (Carroll 1988; Sinclair and Alexander 1987). Sinclair and Alexander (1987) hypothesized that, in reptiles, the body of the quadrate is aligned with the force of the mandible pushing against the skull to effectively resist compression.

The derived feeding apparatus of crocodylians presents a unique opportunity for exploring vertebrate feeding function and evolution. In contrast with the oreoinirostral

(dorsoventrally deep; convex) skulls of early crocodyliforms, those of modern crocodylians are platyrostral (dorsoventrally compressed; flat). The entire skull is dorsoventrally shallow and mediolaterally wide (Figure 1). The quadrate is elongated and swept rostrocaudally, and its body is shallow dorsoventrally. Platyrostry results in substantial mediolateral orientations of many cranial muscles. Crocodylians also generate the highest bite forces measured among vertebrates (Erickson et al. 2003, 2014; Bates & Falkingham 2012). Extinct species such as *Deinosuchus* were likely capable of producing bite forces considerably higher than those from extant taxa (Schwimmer 2002; Erickson et al. 2012).

The powerful loads imposed on the skulls of crocodylians led to the evolution of adaptations to resist and dissipate forces (Langston 1973; Busbey 1995). Extant crocodylians have expanded many intracranial joints. These joints with large, flat articulations are known as scarf joints. Extant crocodylians also possess a secondary bony palate more extensive than that of mammals. The secondary palate has been suggested to resist some of these bending forces in the skull (Langston 1973; Busbey 1995). Finally, the pterygoids of crocodylians are ventrally and rostrocaudally expanded into a robust flange known as the pterygoid buttress (Figure 1; Figure 2). The pterygoid buttress has been suggested to resist medial excursion of the mandible that result from the medial component of adductor force (Iordanksy 1964; Busbey 1995; Porro et al. 2011). The derived morphology and extreme, well-characterized bite force performance of crocodylians make them an intriguing group in which to explore the relationship between skull form and the generation and resistance of cranial forces.

Modeling offers researchers tools with which to test hypotheses of bite force and joint force performance of extant and extinct taxa. *In vivo* bite force data are challenging to obtain, making computational modeling necessary to explore patterns of form and function. Additionally, while bite force data are relatively straightforward (albeit challenging) to obtain experimentally, directly measuring joint forces poses is presently very difficult (Curtis et al. 2010). *In silico* predictions cannot replace *in vivo* measurements as a source of bite force performance data; however, computational methods can be applied more widely. Researchers can model biting under varying conditions of tooth contact, gape, and muscle recruitment. Thus, computational methods are often a researcher's best option for investigating the relationship between morphology, bite force, and resulting cranial forces.

Modeling has been applied to the biomechanics of crocodylian skulls since the 1980s. Early works used two-dimensional static equilibrium lever analyses (Sinclair and Alexander 1987; Busbey 1989; Cleuren et al. 1995). Sinclair and Alexander (1987) used the principles of static equilibrium to estimate bite force at an anterior and posterior position in *Caiman sclerops*, and estimated joint reaction force magnitude and orientation for these bites. The authors concluded that the reaction force experienced by the jaw joints is compressive, decreases in magnitude with more posterior bites, and becomes more ventrally and less caudally orientated. Busbey (1989) found similar orientations of reaction forces at the jaw joint in an individual of *Alligator mississippiensis*. The author found that in crushing bites, joint reaction force is oriented rostradorsally, and that the resultant becomes more vertical as gape decreases. Cleuren et al. (1995) used electromyographic analysis of muscle recruitment and estimated physiological cross-

sectional area (PCSA) to compute bite force and joint forces in an individual of *Caiman crocodilus*. While citing some specific differences in joint reaction force orientation under different orientations of bite force, Cleuren et al. found a pattern generally in accord with previous studies.

Finite element analysis (FEA) was first used to study crocodylian cranial biomechanics by Daniel and McHenry (2001). Using myological data from previous studies (Sinclair and Alexander 1987; Busbey 1989), the authors presented the first hypothesized distributions of stress and strain in the skulls of crocodylians, setting the stage for further such studies. Metzger et al. (2005) used beam modeling and FEA to estimate strain patterns in the skull of *Alligator mississippiensis*, checking predictions against *in vivo* strain data. In one of the first papers to apply biomechanical modeling to several species of crocodylians, McHenry et al. (2006) highlight the importance of the third (i.e., mediolateral) dimension in assessing the biomechanical performance of the crocodylian skull. Interestingly, while this study agreed with prior suggestions that oreinirostral morphologies confer efficient resistance to dorsoventral bending (Busbey 1995), the hypothesis that the platyrostral skull of crocodylians confers torsional resistance was not supported. Rayfield and colleagues (Rayfield et al. 2007; Rayfield and Milner 2008) used FEA to validate the use of extant crocodylians as the living analog for spinosaurid theropod dinosaurs. Finally, Porro et al. (2011, 2013) performed the most comprehensive studies of the biomechanics of the lower jaw of crocodylians to date, incorporating dynamic PCSAs and sutural material properties in the model. These papers integrated beam theory, lever mechanics, and FEA to assess the role of adductor musculature, morphology, bite position, etc. in stress and strain of the mandible.

Whereas most previous modeling studies have investigated the effects of muscle force on cranial forces in the skulls of crocodylians, few have relied on anatomically detailed muscular morphology from an ontogenetic range of animals. The contribution of individual cranial muscles to bite force and joint reaction forces also remains unknown, and the effect of gape on these cranial forces is unexplored. The biomechanical environment of the primary jaw joint in crocodylians has only been considered in a few publications. Furthermore, the biomechanics of the pterygoid buttress are almost entirely unknown. The effects of muscle size and configuration, jaw gape, and bite position on the magnitude and orientation of cranial forces are unknown. Thus, despite the long history of functional analyses of crocodylian crania, our understanding of the biomechanical environment of the head remains unclear.

This study uses cranial morphology, myology, and 3D computational modeling to estimate bite force and joint forces in an ontogenetic series of *Alligator mississippiensis* to explore how cranial musculature loads the skull in static bites. Muscle mapping was informed by dissections, and estimates of PCSA guided calculations of muscle force. These muscle force data were used as input for 3D lever mechanics and finite element analysis (FEA). Bite force was calculated using both methods. However, 3D lever mechanics will be used in modeling reaction force at the pterygoid buttress, and FEA was used for calculating reaction force at the jaw joint.

I hypothesize that my model will generate bite forces consistent with the positively allometric slope Erickson et al. (2003) found. I also hypothesize that my joint reaction forces will scale with a slope equivalent to that of bite force. I hypothesize that jaw joint reaction forces will be aligned with the body of the quadrate. Finally, I

hypothesize that the reaction force at the pterygoid buttress will be of a magnitude comparable with that found at the jaw joint.

MATERIALS AND METHODS

Specimens and Model Construction

Frozen, unpreserved heads were obtained from Rockefeller Wildlife Refuge in Grand Chenier, Louisiana. Skull lengths ranged from 4.8 cm to 33.3 cm. The smallest individual (AL 031; skull length ~4.8 cm) was scanned with a Siemens Inveon MicroCT scanner at the University of Missouri Biomolecular Imaging Center; interslice spacing was 0.083 cm. Other animals data were scanned with a GE LightSpeed VCT computed tomography (CT) scanner at the University of Missouri School of Veterinary Medicine; interslice spacing was 0.5 cm. Figure 3 shows the process of turning CT data into biomechanical models. Stacked images were segmented (Figure 3A) in Avizo 9 (Visualization Sciences Group), and 3D models were created. Models were cleaned and mandibles were manipulated (Figure 3B) in Geomagic Studio 13 (Geomagic, Inc, Research Triangle Park, NC), and meshes were constructed (Figure 3C) of four-noded tetrahedra in Strand7 (G1D Computing Pty Ltd, Sydney, Australia). Finally, muscles were mapped onto the models (Figure 3D). The dimensions of the models are as follows: x is positive in the left lateral direction, y is positive in the dorsal direction, and z is positive in the rostral direction. The mandibles of each model were manipulated to a low gape (“closed;” ~5°) for comparison. The smallest and largest specimens were modeled at both low gape and high gape (“open;” ~30°).

Both methods of calculating cranial forces require accurate estimations of the force of muscular contraction. A muscle generates force in proportion to its physiological cross-sectional area (PCSA). PCSA is a function of muscle volume, fiber length (modeled as a fraction of the total muscle length), and muscle pennation angle, as defined in Equation 1 (Sacks and Roy 1982):

$$PCSA = \frac{V}{l_f} \cdot \cos(\theta) \quad (1)$$

where V is volume of the muscle, l_f is the fiber length of the muscle, and θ is the angle of pennation. PCSA may also be defined by dividing muscle mass by density. However, in order to make comparisons with fossil taxa, the muscle attachment definition was used for this study. Muscle volumes were estimated by modeling each muscle as a frustum, or a cone with its apex cut off parallel with its base. Equation 2 describes the volume of a frustum:

$$V = \frac{l_M}{3} \cdot (A_{or.} + A_{ins.} + \sqrt{A_{or.} \cdot A_{ins.}}) \quad (2)$$

where l_M is the length of the muscle, $A_{or.}$ is the surface area of the origin of the muscle, and $A_{ins.}$ is the surface area of the insertion. Muscle attachment sites were mapped onto finite element models in Strand7. Due to small variations in mesh construction, muscle attachment areas were not always perfectly symmetrical, but never differed more than 5%. Dissections and reference to the literature guided muscle mapping (Iordansky 1964, 2000; Schumacher 1973; Busbey 1989; Holliday and Witmer 2007; Holliday et al. 2013). The ratio between PCSA and force produced is known as specific tension, described in Equation 3:

$$\mathbf{F}_M = PCSA \cdot T_{specific} \quad (3)$$

where F_M is muscle force, and T_{specific} is specific tension. Pennation, fiber length, and specific tension data are from Porro et al. (2011). Unilateral, left-sided, static, crushing bites were modeled. In the absence of detailed muscle recruitment data, muscles were assumed to contract simultaneously and maximally, as suggested by Busbey (1989) and Cleruen et al. (1995). For each specimen, an anterior, an intermediate, and a posterior bite were modeled. The rostral and caudal bites were on the most mesial and most distal tooth on the dentary. The intermediate bites were on the most prominent tooth on the dentary.

Myology

All muscle terminology is after Holliday and Witmer (2007). In the present study, muscles modeled were m. Adductor Mandibulae Externus Superficialis (mAMES), m. Adductor Mandibulae Externus Medialis (mAMEM), m. Adductor Mandibulae Externus Profundus (mAMEP), m. Adductor Mandibulae Posterior (mAMP), m. Pseudotemporalis Superficialis (mPSTs), m. Pseudotemporalis Profundus (mPSTp), m. Pterygoideus Dorsalis (mPTd), m. Pterygoideus Ventralis (mPTv), and m. Depressor Mandibulae (mDM). Figure 4 illustrates bony attachment sites of cranial muscles in this study. In extant crocodylians, most muscles have substantial mediolateral components (mAMEM, mAMEP, mPSTp), rostrocaudal components (mPTd), or both (mAMES, mAMP, mPSTs, mPTv, mDM). While mPSTp was included in muscle maps, its contribution to moments about joint axes and therefore forces proved trivial and it will not be included in analyses.

Joints

This study measures the forces at two craniomandibular joints, the jaw joint, and the contact between the pterygoid buttress and the mandible, or the pterygomandibular joint (PMJ; Figure 1; Figure 2). The crocodylian jaw joint is the ancestral craniomandibular contact between the quadrate and the articular. The quadrate is elongated and swept rostrocaudally, and its body is shallow dorsoventrally, with a gentle ventrocaudal slope. Some authors have suggested that the joint reaction force should align with the body of the quadrate to absorb stress; any other dorsoventral orientation would result in bending moments of the quadrate (Sinclair and Alexander 1987). At its articulation, the quadrate bears a biconvex surface, fitting into the saddle-shaped articular fossa of the articular. The surangular forms a “lip” on the lateral rim of the articular fossa. The pterygomandibular joint is a novel craniomandibular articulation in evolved in crocodyliformes. The PMJ is built by the mandible and the pterygoid flange on the cranium. In crocodyliformes, the pterygoid bone extends further ventrally than in most sauropsids, and is rostrocaudally expanded. The PMJ has been hypothesized to resist medial excursion of the mandibles in biting (Busbey 1995).

3D Lever Analysis

In lever systems, force is transmitted by rotation of an element about an axis. An input force acting at a distance imparts a moment of force (a measure of rotational tendency) about an axis. An object at a distance from the axis resisting this rotational moment will experience an output force. Equation 4 shows the relationship between input force and distance and output force and distance:

$$\mathbf{r}_{axis} \cdot (\mathbf{r}_{in} \otimes \mathbf{F}_{in}) = M = \mathbf{r}_{axis} \cdot (\mathbf{r}_{out} \otimes \mathbf{F}_{out}) \quad (4)$$

where \mathbf{r}_{axis} is the vector that describes the axis of rotation, \mathbf{r}_{in} is the moment arm that perpendicularly connects the input force and the axis of rotation, \mathbf{F}_{in} is the vector of input force, M is the moment of force about the rotational axis, \mathbf{r}_{out} is the moment arm that perpendicularly connects the axis of rotation and the point of resistance, and \mathbf{F}_{out} is the vector of output force. In the feeding apparatus, cranial muscles provide the input force for rotation (\mathbf{F}_M). (The muscle force was not a single vector as in most previous studies; see below.) The perpendicular distance from the muscle force vector to the axis of rotation is known as the moment arm of the muscle (\mathbf{r}_M). Output forces calculated with lever systems acts perpendicularly to the plane containing the axis of rotation and the output moment arm. In the present study, 3D lever mechanics were used to calculate two output forces: bite force (\mathbf{F}_B) and PMJ force (\mathbf{F}_{PMJ}). Equations 5 shows this calculation for the jaw joint axis:

$$\mathbf{r}_{JJA} \cdot (\mathbf{r}_M \otimes \mathbf{F}_M) = M = \mathbf{r}_{JJA} \cdot (\mathbf{r}_B \otimes \mathbf{F}_B) \quad (5)$$

where \mathbf{r}_{JJA} is the jaw joint axis (defined as the vector passing through the middle of the joint surfaces of the left and right articular bones), \mathbf{r}_M is the moment arm of muscle force, \mathbf{F}_M is muscle force, M is the moment about the jaw joint axis, \mathbf{r}_B is the position vector of bite force, and \mathbf{F}_B is bite force. Equation 6 shows this calculation for the PMJ axis:

$$\mathbf{r}_{PMJA} \cdot (\mathbf{r}_M \otimes \mathbf{F}_M) = M = \mathbf{r}_{PMJA} \cdot (\mathbf{r}_{PMJ} \otimes \mathbf{F}_{PMJ}) \quad (6)$$

where \mathbf{r}_{PMJA} is the PMJ axis (defined as a vector passing vertically through the middle of the joint surface of each articular bone), \mathbf{r}_M is the moment arm of muscle force, \mathbf{F}_M is muscle force, \mathbf{r}_{PMJ} is the moment arm of PMJ force, and \mathbf{F}_{PMJ} is the PMJ force. Figure 5 shows rotational axes used for this study. Lever mechanics are illustrated in Figure 6 for

the calculation of bite force at a rostral tooth. For visual clarity, only mAMP is shown in Figure 6.

In this study, the total muscle force was distributed over the surface area of attachment of the insertion. Each face of a tetrahedral element belonging to a muscle insertion bore a portion of the total force, directed at the centroid of the muscle origin. The computational toolkit Boneload (Grosse et al. 2007) was used for calculating moments about axes and to distribute muscle forces across attachment sites. Boneload was originally used in modeling bite forces in phyllostomid bats (Grosse et al. 2007), and its predictions were well-supported by *in vivo* measurements (Davis et al. 2010; Santana et al. 2010). Boneload uses the geometry of muscle attachments and user-defined muscle forces calculate moments about a user-defined axis of rotation.

Finite Element Analysis

To calculate bite forces and reaction forces at the jaw joint, finite element models (FEMs) of the mandible of each specimen were made from CT data. Bite force was also calculated using FEA to validate estimates from 3D lever mechanics. To calculate forces using FEA, muscle attachment sites were mapped onto a solid tetrahedral mesh of each skull, as described above. Boneload was used to distribute calculated muscle forces across each muscle attachment site. These forces were used to load the FEM. The FEA software then calculates reaction forces at each reaction point (both jaw joints and the bite point) needed to restore static equilibrium. FEA is therefore most appropriate for the modeling of static, crushing bites, such as those crocodylians use to process prey (Busbey 1989; Cleuren et al. 1992). Material properties of alligator femoral cortical bone were

assigned to all elements of the FEM. Methods described by Strait et al. (2005) were followed to assign constraints. A single node in the middle the joint surface of each articular bone was constrained in all three translational and all three rotational degrees of freedom. A single node at the tip a posterior, an intermediate, or an anterior tooth was also constrained in all degrees of freedom. Because FEA provides force orientations in addition to magnitudes (F_{sum}), the component of force in each dimension will be reported (mediolateral, F_x ; dorsoventral, F_y ; rostrocaudal, F_z).

Comparison of Calculated Bite Forces with *In Vivo* Data

Finally, total bite forces and joint forces calculated using both 3D lever mechanics and FEA were compared with *in vivo* bite force data from Erickson et al. (2003; 2014) to test the validity of the model. Erickson and colleagues measured *in vivo* maximum bite force in an ontogenetic series of *Alligator mississippiensis*. To assess how well calculated bite forces matched *in vivo* data, a reduced major axis regression analysis of bite forces and skull length was conducted using R (R Core Team). The slope of the regression lines of calculated data were compared to those reported by Erickson et al. (2003).

RESULTS

All results will be reported in ascending order of skull length. AL 031: 4.8 cm.
AL 622: 9.9 cm. AL 612: 20.3 cm. AL 024: 26.9 cm. AL 700: 33.3 cm.

Muscles and Models

Model size ranged from 892256 to 1989413 four-noded tetrahedra. Reduced major axis regression of muscle length, volume, force, against cranial length showed that all parameters scaled to isometry in all muscles with the exception of mAMEP, in which muscle volume and force scaled with slight negative allometry (data not shown). Table 1 shows reconstructed muscle force, and Table 2 shows the proportion each muscle contributes to total muscle force. Table 2 shows moments about the jaw joint axis for low gape.

Bite Force

Bite force estimation with 3D lever mechanics and FEA yielded similar results. Table 3 shows the moment each cranial muscle contributed to mandibular adduction, and Table 4 shows the proportion of each muscle to total moments about the jaw joint axis. Table 5 shows bite force data calculated with both methods. Table 8 shows the directional components of bite forces calculated with FEA. For posterior bites at low gape, bite forces calculated with lever mechanics were 40.8 N, 133 N, 349 N, 844 N, and 1170 N, and bite forces calculated with FEA were 36.6 N, 120 N, 298 N, 726 N, and 1310 N. For intermediate bites at low gape, bite forces calculated with lever mechanics were 30.2 N, 95.6 N, 254 N, 628 N, and 884 N, and bite forces calculated with FEA were 26.7 N, 84.0 N, 220 N, 501 N, and 882 N. For anterior bites at low gape, bite forces calculated with lever mechanics were 18.3 N, 61 N, 163 N, 417 N, and 571 N, and bite forces calculated with FEA were 26.8 N, 91.7 N, 241 N, 409 N, and 759 N.

For posterior bites at high gape, bite forces calculated with lever mechanics were 33.5 N and 984 N, and bite forces calculated with FEA were 37.0 N and 1340 N. For intermediate bites at high gape, bite forces calculated with lever mechanics were 27.5 N and 676 N, and bite forces calculated with FEA were 26.3 N and 901 N. For anterior bites at high gape, bite forces calculated with lever mechanics were 13.5 N and 426 N, and bite forces calculated with FEA were 27.0 N and 736 N.

Forces predicted with 3D lever mechanics were higher than those predicted with FEA for posterior bites at low gape, with the exception of the largest specimen. Forces predicted with 3D lever mechanics were higher than those predicted with FEA for all intermediate bites at low gape. In contrast, forces calculated with FEA were higher than those predicted with 3D lever mechanics for anterior bites at low gape. Forces calculated with FEA were also higher for all bites at high gape with the exception of the intermediate bite of the smallest individual. Neither method generated bite forces that scaled significantly differently from isometry. When compared to data measured *in vivo* by Erickson et al. (2003), two things were noted. First, computational models in the present study predict lower bite forces than those reported by Erickson et al. (2003). Second, the regression slope of calculated data is lower than that reported by Erickson and colleagues, who reported significant positive allometry when maximum force was regressed against skull length. Potential reasons for these discrepancies will be discussed later.

Joint Forces

Joint force data are summarized in Table 6 (jaw joint) and Table 7 (PMJ). Table 8 includes directional components of jaw joint force. Magnitudes of reaction forces at the left jaw joint for posterior bites at low gape were 39.7 N, 131 N, 434 N, 823 N, and 1490 N. Magnitudes of reaction forces at the right jaw joint for posterior bites at low gape were 40.4 N, 141 N, 465 N, 879 N, and 1370 N. Magnitudes of reaction forces at the left jaw joint for intermediate bites at low gape were 37.0 N, 144 N, 467 N, 885 N, and 1640 N. Magnitudes of reaction forces at the right jaw joint for intermediate bites at low gape were 38.7 N, 140 N, 455 N, 881 N, and 1350 N. Magnitudes of reaction forces at the left jaw joint for anterior bites at low gape were 33.1 N, 143 N, 435 N, 840 N, and 1460 N. Magnitudes of reaction forces at the right jaw joint for anterior bites at low gape were 38.8 N, 142 N, 454 N, 848 N, and 1340 N. For posterior bites at low gapes, the balancing side jaw joint was always loaded in compression, and the working side jaw joint was loaded in tension. Anterior bites at low gapes produced only compressive reaction forces at the jaw joints.

Magnitudes of reaction forces at the left jaw joint for posterior bites at high gape were 40.0 N and 1480 N. Magnitudes of reaction forces at the right jaw joint for posterior bites at high gape were 40.0 N and 1350 N. Magnitudes of reaction forces at the left jaw joint for middle bites at high gape were 36.7 N and 1620 N. Magnitudes of reaction forces at the right jaw joint for middle bites at high gape were 38.3 N and 1320 N. Magnitudes of reaction forces at the left jaw joint for anterior bites were 32.9 N and 1390 N. Magnitudes of reaction forces at the right jaw joint for anterior bites were 38.4 N and 1300 N.

Magnitudes of reaction forces at the left PMJ for bites at low gape were 19.1 N, 91.6 N, 128 N, 507 N, and 995 N. Magnitudes of reaction forces at the right PMJ for bites at low gape were 12.8 N, 57.6 N, 105 N, 496 N, and 896 N. Because PMJ calculations do not involve specifying a bite point, anterior and posterior bites were not specified.

Statistical Analyses

Tables 11, 12, and 13 show the results of reduced major axis regression analysis for posterior, intermediate, and anterior bites. Right jaw joint force for all bite positions and FEA bite force for anterior bites scaled to slight negative allometry. All other calculated cranial forces did not scale significantly different from isometry.

DISCUSSION

My modeling approach yields consistent results. At low gape, magnitudes of total bite forces calculated with FEA are all less than ~20% different from those calculated with 3D lever mechanics. At high gape, FEA and 3D lever mechanics differ up to 33%. Bites in equivalent positions also produced bite forces of similar orientations in all animals. Moreover, bites at differing locations along the tooth row show distinct orientations. Calculated bite forces were lower than those reported by Erickson et al. (2003) for similarly-sized animals, and scaled to isometry rather than the positive allometry found *in vivo*.

Effects of Gape and Bite Position

Bite force calculated from 3D lever mechanics always decreased in anterior bites relative to posterior bites. Weaker anterior biting is a consequence of a longer out lever (output moment arm) (Herring and Herring 1974; Dumont and Herrel 2003). Because FEA provides the components of force in each dimension, the effect of bite position on force orientation was observable. Teeth in posterior bites experience the highest total bite force (F_{sum}) as well as highest dorsoventral forces (F_y). Bite force is oriented most vertically in posterior bites. Relative to posterior bites, teeth in intermediate bites have lower total bite force and lower dorsoventral bite force. For three of the animals modeled at low gape, the magnitude of total bite force is lowest for the middle bite position, rather than for the anterior position, as would be expected. However, teeth in anterior bites experience the lowest dorsoventral bite force and the highest rostrocaudal force. The bite force resultant is the least vertical for anterior bites. Indeed, in anterior bites, FEA suggests that the majority of bite force magnitude is rostrocaudally oriented.

Interestingly, anterior and posterior bites experience a laterally directed component of force, while middle bites experienced a medially directed force. Figure 7 summarizes this pattern for the largest individual (AL 700; skull length ~33.3 cm). Patterns in the magnitude of bite force therefore obscure patterns of bite force components.

The pattern for bite force at high gapes is complex. At high gape, bite forces calculated with 3D lever mechanics are lower than bites at corresponding teeth at low gape. This is the expected pattern, as the moment arm of jaw muscles decreases at high gape. The sum of moments about the jaw joint axis (and therefore bite force) at high gape were 73.3% and 74.7% of the sum at low gape (Table 3). However, when calculated with

FEA, the magnitude of total bite force shows little change with gape; total bite force calculated for high gape and low gape differed by less than 3%. While magnitudes are equivalent between low and high gape, the distribution of force among the three dimensions is different. Bites at high gape experienced more rostrocaudal forces and lower dorsoventral forces relative to low gape bites at equivalent teeth.

Comparisons with *In Vivo* Bite Force Data

There are several likely causes for the discrepancy between calculated data and the *in vivo* data from Erickson et al. (2003). These causes may be divided into submaximal model performance and behavioral differences between modeled bites and *in vivo* bites. Crocodylians have an extensive cranial tendinous skeleton (Iordansky 1964, 2000; Schumacher 1973; Busbey 1989). Some muscles, such as m. Pterygoideus Ventralis, have extensive attachments to the cranial tendons. Because tendons are difficult to see on CT scans, tendinous attachments were not included in muscle maps. Therefore, the force of muscular contraction for some muscles in these models were presumably below the *in vivo* maximum. Contrast-enhanced CT imaging of soft tissues could allow the inclusion of the tendon skeleton in future models of extant taxa.

This model's concept of bite force is not the same as that of Erickson et al. (2003). Our modeling techniques mimicked static, crushing bites. However, Erickson et al.'s (2003) *in vivo* bite force data from *Alligator mississippiensis* were obtained from rapid jaw closure. Erickson et al. (2003) reported the maximum force during "aggressive, snapping" bites. Therefore, the peak force reported by these authors was likely an impact force resulting from rapid mandibular deceleration. Daniel and McHenry (2001)

suggested that “dynamic loading due to rapid deceleration” likely plays a role in maximal forces experienced by the skull. Because the present study modeled static, crushing bites, which have no contribution from impact forces, estimated maximum bite forces are presumably below peak forces experienced by the mandibles. Furthermore, Cleuren et al. (1992) reported that larger caimans elevate the cranium relative to a horizontal plane and depress it during biting, suggesting that not only the mandible but also the cranium has independent impact forces. Videos of alligator feeding events also capture this behavior (<http://videos.howstuffworks.com/discovery/33170-crocodile-feeding-frenzy-gator-jaws-video.htm>).

The finding of our isometric slope also stands in contrast to *in vivo* studies of bite force in alligators, which scaled with positive allometry. Pfaller et al. (2011) found that snapping turtle jaw muscles increase in pennation during ontogeny, resulting in positively allometric changes in overall bite force, independent of geometric or skeletal changes. In this study we assume constant pennation and therefore a constant PCSA for a given muscular size and shape; if this assumption is violated, muscle forces could potentially be underestimated. Furthermore, Busbey (1989) reported that some of the adductor muscles of *Alligator mississippiensis* had complex arrangements of fiber architecture, with some muscles having multiple pennation regimes within a single belly. More data on the ontogeny of muscle fiber architecture and histochemistry are necessary to better model muscle forces.

Joint Forces

Balancing and working side joint reaction forces are of comparable magnitudes for all bites, but show distinct orientations. In posterior bites, balancing side joint reaction forces are compressive, while working side forces are tensile. This pattern was found by Metzger et al. (2003). Busbey (1989) noted that m. Depressor Mandibulae is active during the closing phase of biting. The author suggests that this activity functions to stabilize the jaw joint; our findings support this interpretation. Metzger et al. (2003) suggested submaximal recruitment of balancing side muscles prevented tensile dislocation of the jaw joint. Bramble (1978) also suggested that some mammals modulate muscle force to control tensile forces, which are thought to pose a risk to joint integrity. Metzger et al. (2003) alternatively suggest that the crocodylian jaw joint is designed to avoid dislocation. In anterior bites, the distinct loading of the working and balancing jaw joints is replaced by compressive forces at both jaw joints. Both compressive and tensile reaction forces acting at the jaw joint become more vertical in posterior bites.

Jaw joints also experienced laterally directed reaction forces in all bites, presumably due to the quadratus resisting the medial component of adductor muscle force. The morphology of the jaw joint may reflect this; the muscle scar of the lateral collateral ligaments on the surangular forms a lateral lip for the articular fossa. This may help resist laterally oriented reaction forces at the jaw joint. Surprisingly, the lateral component of joint reaction force was the largest for all bites, and rose even higher for anterior bites. For every anterior bite, the lateral component was larger for the working side jaw joint. However, no clear pattern exists for the balancing side jaw joint. The reaction forces experienced by the PMJ imply that the laterally directed forces found in this study are

artefacts brought by limitations of our modeling approach. The PMJ force was on average 54% of the mediolateral component of the jaw joint reaction force. The PMJ has been suggested to play a role in stabilizing the mandible, preventing medial excursion (Busbey 1995; Porro et al., 2011) and emerging data suggest the PMJ may be a fully-formed second craniomandibular joint with a sesamoid similar in form to the mammalian temporomandibular joint (Tsai and Holliday, 2011; Holliday et al. 2015).

Application to Extinct Taxa

The 3D modeling approaches used in this study may be applied to the fossil record. Because this technique uses the area of muscle attachment site rather than the weight of dissected muscles to estimate PCSA, it can be used to make accurate estimates of muscle force, moments about axes, and resulting forces in extinct animals. Study of osteological correlates and extant relatives (Holliday 2009) can constrain hypothesized attachment location and extent. Functional comparisons with extant relatives can also inform inferences about other myological data, such as pennation angle and fiber length. However, general parameters of the specificity typically available to paleontologists were used.

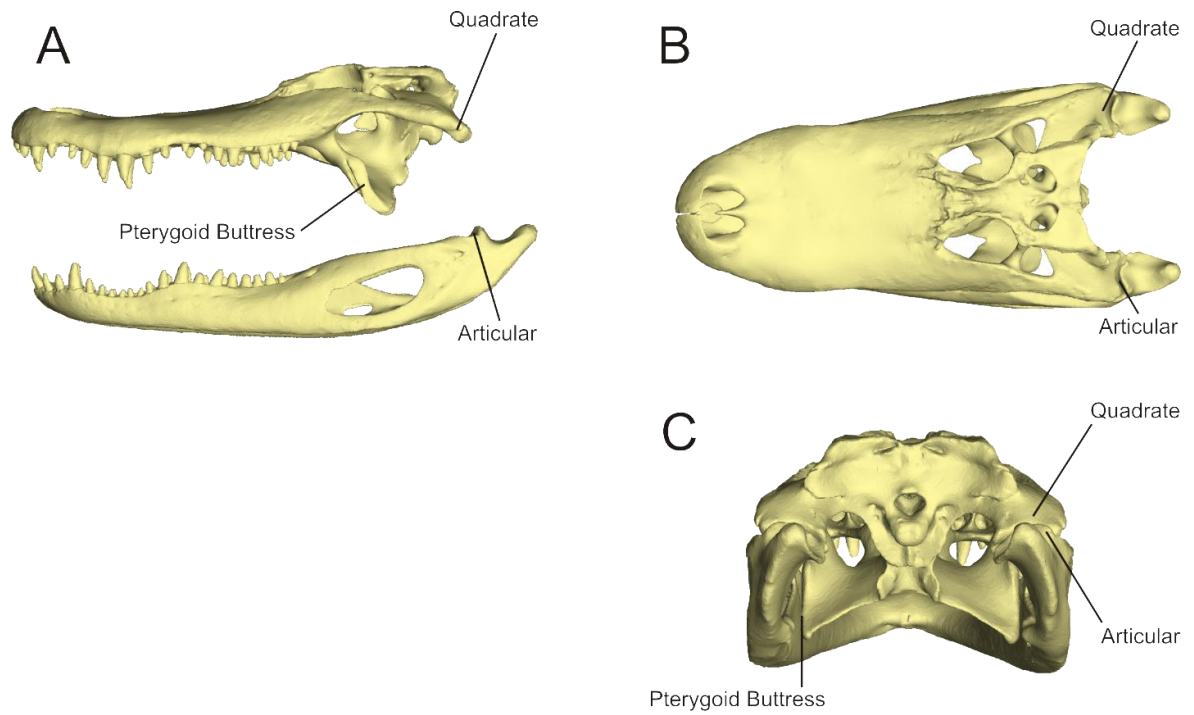
In contrast to the platyrostral skulls of crocodylians, the earliest members of crocodylian-line archosaurs had orienorsotral skulls, such as the rauisuchian *Postosuchus* (Chatterjee 1985) and the sphenosuchian *Sphenosuchus* (Walker 1990). In these animals, the skull is dorsoventrally deep and mediolaterally narrow. The quadrate was generally dorsoventrally oriented, though Busbey (1995) noted a slight posterior rotation of the quadrates. The evolution of the crown group therefore involved substantial reorientation

of adductor muscles from the primitive condition. The deep, narrow skull permitted more efficient insertion of muscles onto the mandible, lengthening the moment arm. The transformation from orienorostral to platyrostral presumably required crocodylians to evolve higher mass or pennation of adductor muscles to achieve equivalent bite forces to their fossil ancestors. These early ancestors also likely possessed some degree of cranial kinesis, and their skulls were less sutured than in modern forms. This suggests that the evolution of the modern crocodylian skull involved a reduction in kinetic potential, possibly permitting the evolution of powerful bite forces.

CONCLUSIONS

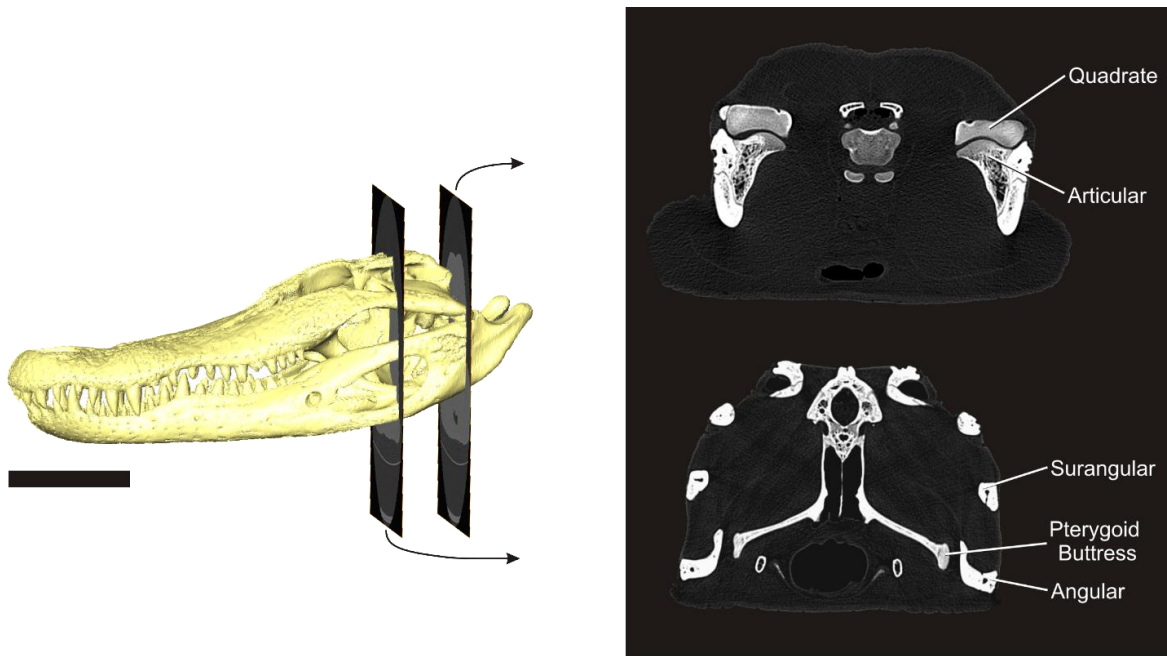
This study is one of the first to use both 3D lever mechanics and FEA to investigate the production of cranial forces in an ontogenetic range of *Alligator mississippiensis*. The use of anatomically accurate muscle attachment is key to the success of the models, and the good agreement between the two methods lends support to these techniques. The modeling techniques in this study can be used to assess the effect of changing muscle size and orientation during the evolution of the modern crocodylian skull. Key features of the crocodylian skull may have permitted novel muscular morphologies. These methods will allow researchers to test hypotheses linking boney features such as the loss of kinesis, secondary palate, scarf joints, and the pterygoid buttress with muscular innovations, such as generally enlarged adductor mass, laterally inserting m. Pterygoideus Ventralis, and the extensive cranial tendinous skeleton.

Figure 1.



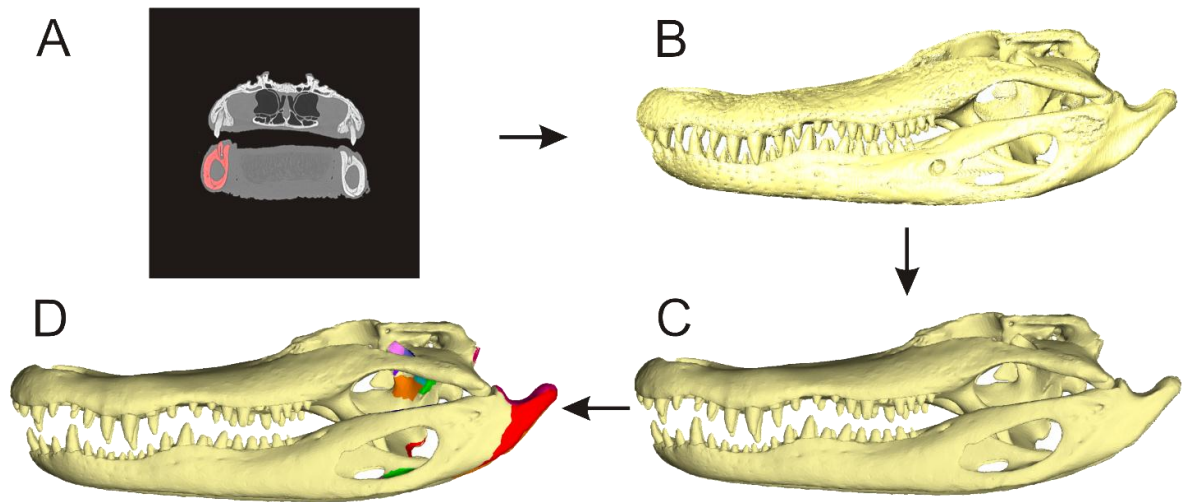
Skull of *Alligator mississippiensis*. The quadrate and articular form the jaw joint; the pterygoid buttress abuts the coronoid, surangular, and angular on the medial side of the mandible. A) Left lateral view. B) Dorsal view. C) Caudal view.

Figure 2.



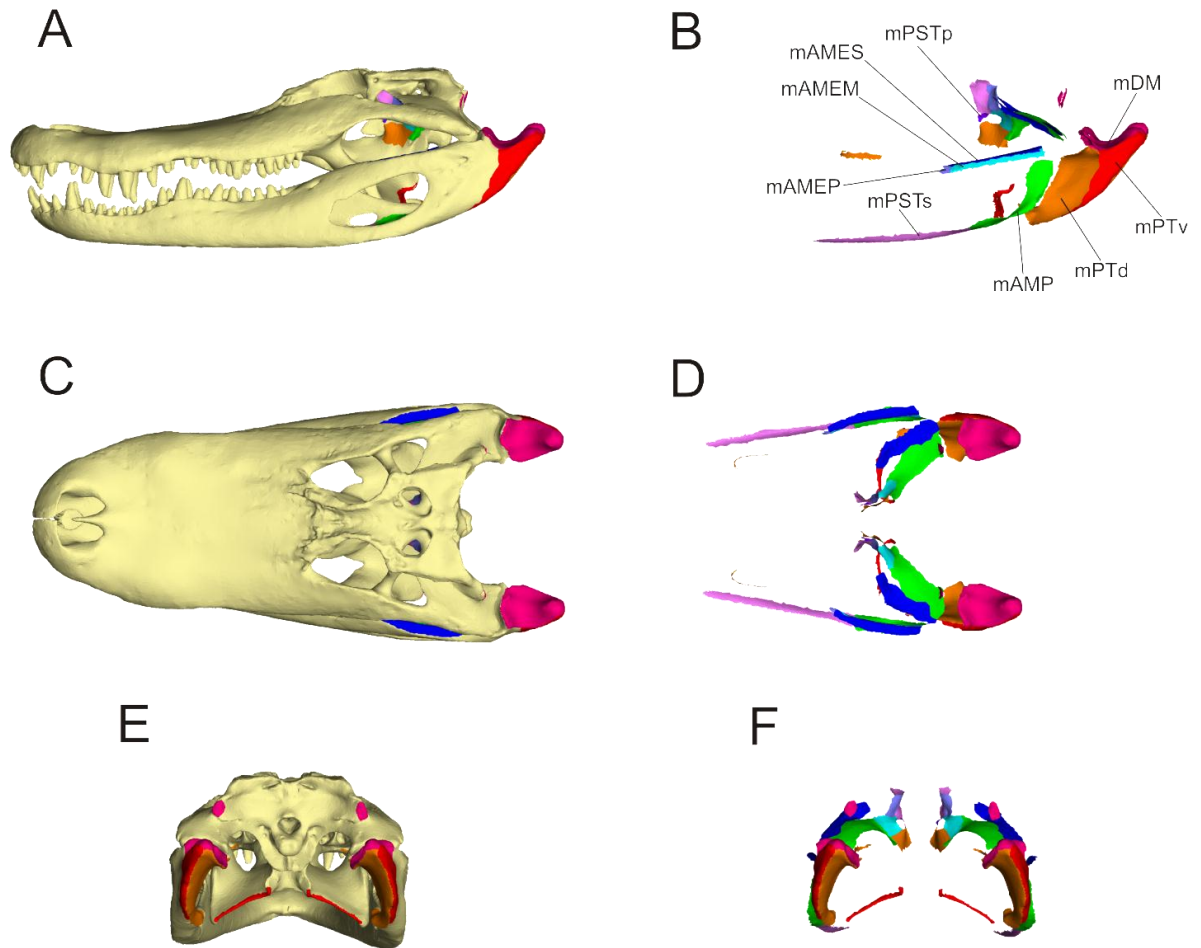
Frontal sections through the jaw joint (top) and PMJ (bottom) of *Alligator mississippiensis*, specimen AL 700. Scale bar is 10 cm.

Figure 3.



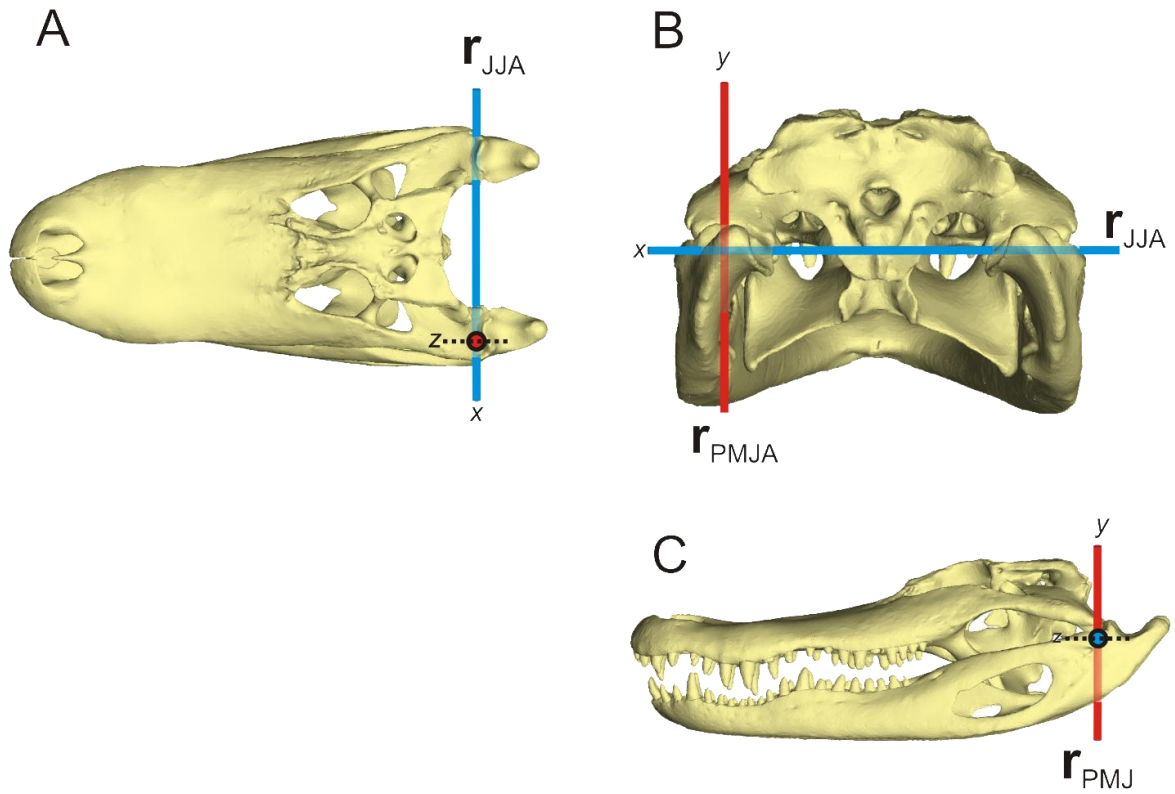
Work flow of making a mapped model of skull. Clockwise from top-left: A) Segmenting cranium and mandible from CT data. B) Model cleaning and manipulation. C) Creation of tetrahedral mesh. D) Muscle mapping.

Figure 4.



Muscle attachment sites on skull of AL 700. A, C, E show muscle attachment sites on the skull; B, D, and F show only attachments. A,B) Left lateral view. B,C) Dorsal view. E, F) Caudal view. Muscle names: m. Adductor Mandibulae Externus Superficialis (mAMES), m. Adductor Mandibulae Externus Medialis (mAMEM), m. Adductor Mandibulae Externus Profundus (mAMEP), m. Adductor Mandibulae Posterior (mAMP), m. Pseudotemporalis Superficialis (mPSTs), m. Pseudotemporalis Profundus (mPSTp), m. Pterygoideus Dorsalis (mPTd), m. Pterygoideus Ventralis (mPTv), m. Depressor Mandibulae (mDM)

Figure 5.



Axes of rotation used for 3D lever mechanics. r_{JJA} = jaw joint axis. r_{PMJA} = pterygomandibular joint axis. Dimensions are labeled on the positive side of each axis. A) Dorsal view. B) Caudal view. C) Left lateral view.

Figure 6.

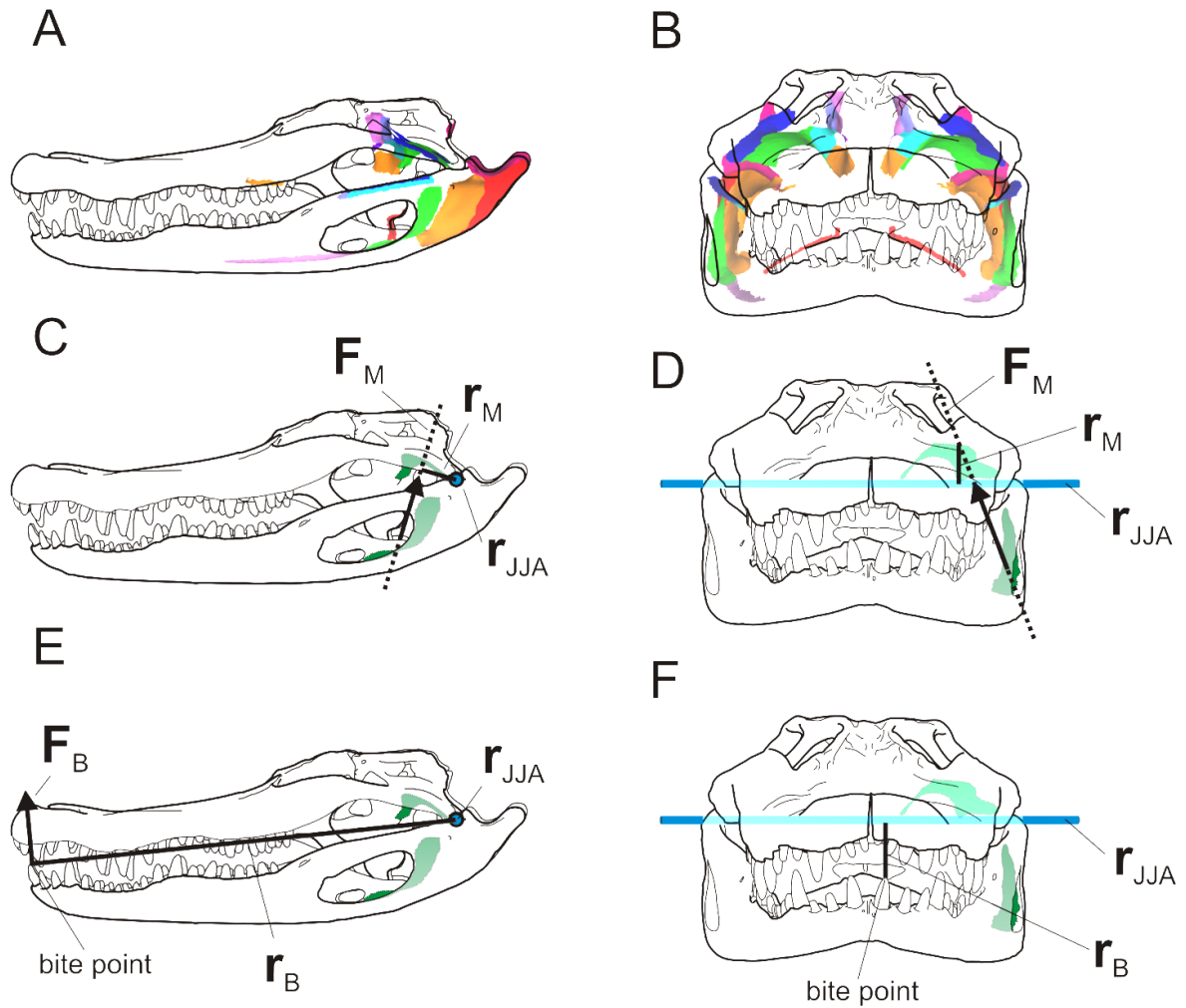


Illustration of calculation of moment about jaw joint axis and bite force. Only an anterior bite at low gape is shown. For clarity, the calculation is shown only for m. Adductor Mandibulae Posterior. A,C,E) Left lateral view. B,D,F) Rostral view. A,B) Muscle maps *in situ*. C,D) Calculation of moment about jaw joint axis for mAMP. F_M = muscle force, r_M = muscle moment arm, r_{JJA} = jaw joint axis. E,F) Calculation of bite force. r_B = bite point moment arm, F_B = bite force. (Note: in Figure 6F, F_B lies in the same plane as r_B , and is not shown.)

Figure 7.

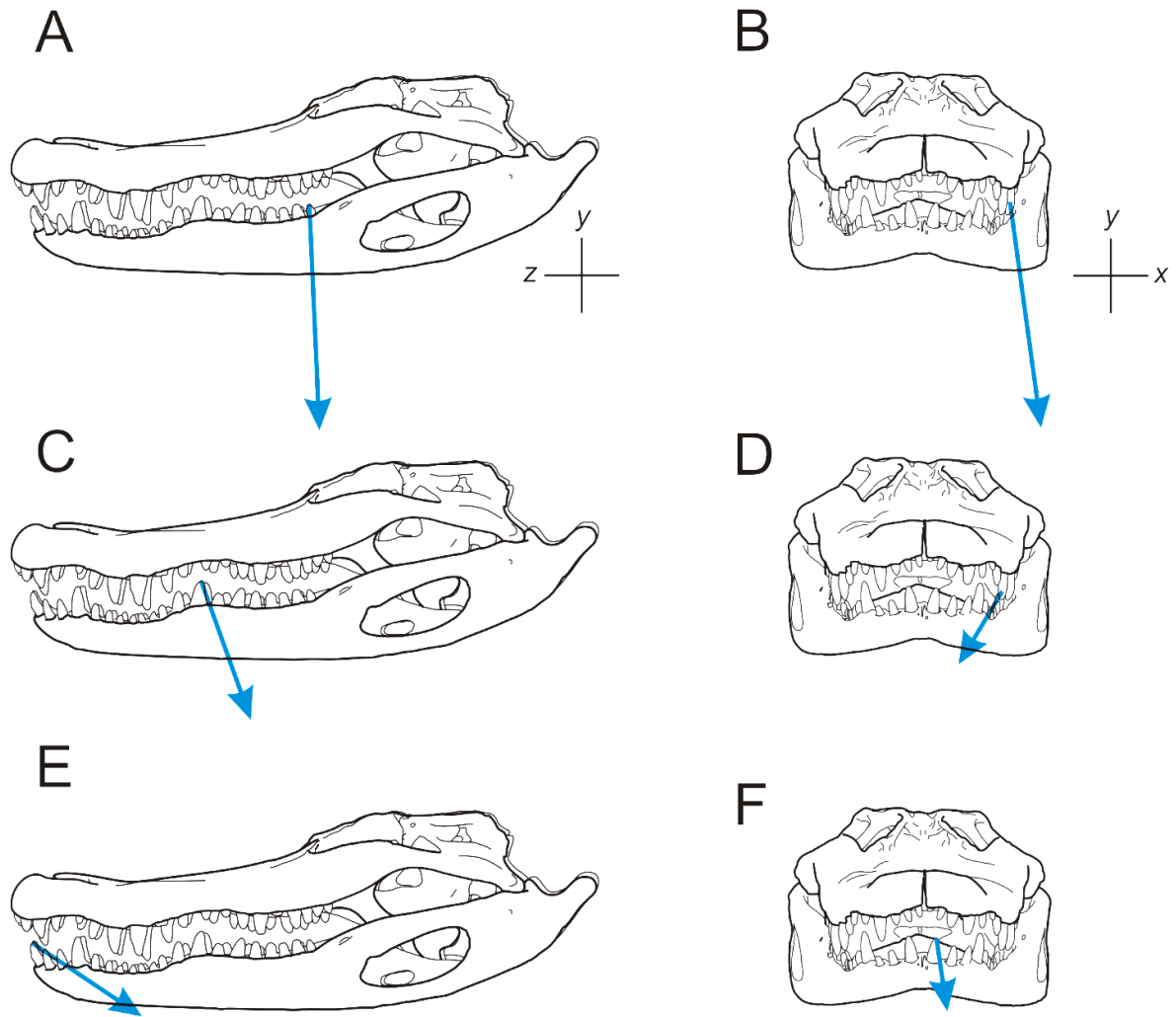


Illustration showing changing bite force orientation for low gape bites for largest specimen (AL 700). Vectors are drawn to scale. Dimensions are labeled in the positive direction. A,C,E) Left lateral view. B,D,F) Rostral view. A,B) Posterior bite. C,D) Intermediate bite. E,F) Anterior bite.

Table 1. Forces of jaw muscles of *Alligator mississippiensis* calculated by estimating PCSA by frustum muscle modeling.

Specimen	AL 031	AL 622	AL 612	AL 024	AL 700
Skull Length (cm)	4.8	9.9	20.3	26.9	33.3
	Forces (N)				
L mAMES	5.57	32.6	72.8	154	287
R mAMES	5.44	31.6	70.5	160	299
L mAMEM	4.29	12.5	31.1	45.2	120
R mAMEM	4.22	12.1	32.2	46.3	117
L mAMEP	2.30	5.55	15.2	35.3	34.3
R mAMEP	2.26	5.13	15.2	33.1	33.3
L mAMP	28.4	110	309	659	1150
R mAMP	29.3	107	300	652	1040
L mPSTs	11.7	34.5	85.9	197	361
R mPSTs	11.3	34.5	87.9	197	351
L mPTd	41.4	131	425	1020	1560
R mPTd	38.4	135	427	1030	1590
L mPTv	6.71	29.3	68.5	172	323
R mPTv	6.23	30.0	75.0	177	332
L mDM	9.66	24.1	105	330	340
R mDM	9.37	25.5	111	326	336

Table 2. Contribution of each jaw muscle to total muscle force.

Specimen	AL 031	AL 622	AL 612	AL 024	AL 700
Skull Length (cm)	4.8	9.9	20.3	26.9	33.3
Muscle	Proportion				
L mAMES	2.57%	4.28%	3.26%	2.94%	3.47%
R mAMES	2.51%	4.15%	3.16%	3.06%	3.61%
L mAMEM	1.98%	1.64%	1.39%	0.86%	1.45%
R mAMEM	1.95%	1.60%	1.44%	0.88%	1.41%
L mAMEP	1.06%	0.73%	0.68%	0.67%	0.42%
R mAMEP	1.04%	0.67%	0.68%	0.63%	0.40%
L mAMP	13.1%	14.5%	13.9%	12.6%	13.8%
R mAMP	13.5%	14.1%	13.5%	12.5%	12.6%
L mPSTs	5.39%	4.53%	3.85%	3.77%	4.36%
R mPSTs	5.21%	4.53%	3.94%	3.77%	4.24%
L mPTd	19.1%	17.25%	19.1%	19.5%	18.9%
R mPTd	17.7%	17.75%	19.1%	19.6%	19.2%
L mPTv	3.10%	3.86%	3.07%	3.30%	3.91%
R mPTv	2.88%	3.94%	3.36%	3.39%	4.02%
L mDM	4.46%	3.17%	4.70%	6.30%	4.11%
R mDM	4.33%	3.36%	4.98%	6.24%	4.07%

Table 3. Muscle moments about jaw joint axis (r_{jj}) calculated with 3D lever mechanics.

Specimen	AL 031	AL 622	AL 612	AL 024	AL 700		AL 031	AL 700
Skull Length (cm)	4.8	9.9	20.3	26.9	33.3		4.8	9.9
	Moments (N*m)							
Muscle	Closed						Open	
L mAMES	0.0340	0.414	1.58	4.77	9.47		0.0316	9.75
R mAMES	0.0379	0.409	1.57	5.16	9.06		0.0354	10.6
L mAMEM	0.0251	0.124	0.620	1.15	3.09		0.0260	3.67
R mAMEM	0.0250	0.123	0.616	1.24	2.88		0.0266	3.86
L mAMEP	0.0259	0.113	0.531	1.60	1.79		0.0240	1.930
R mAMEP	0.0261	0.109	0.496	1.54	1.77		0.0240	2.00
L mAMP	0.113	0.989	5.12	17.0	26.0		0.0926	21.7
R mAMP	0.126	0.901	4.63	16.3	23.7		0.102	22.8
L mPSTs	0.162	0.846	3.68	11.2	24.4		0.148	24.2
R mPSTs	0.193	0.883	3.74	11.6	23.7		0.142	24.2
L mPTd	0.166	1.05	6.35	24.9	34.5		0.106	13.3
R mPTd	0.122	0.966	5.20	23.2	33.0		0.0589	17.5
L mPTv	0.0235	0.244	0.860	3.11	8.15		0.0142	4.34
R mPTv	0.0235	0.201	0.899	3.38	8.55		0.0152	5.74
L mDM	9.66	24.1	105	330	340		-0.0355	-8.98
R mDM	9.37	25.5	111	326	336		-0.0377	-8.34

Table 4. Contribution of each muscle to total adducting moments about jaw joint axis (r_{1j}) calculated with 3D lever mechanics. (Note: m. Depressor Mandibulae is not included in this calculation.)

Specimen	AL 031	AL 622	AL 612	AL 024	AL 700		AL 031	AL 700
Skull Length (cm)	4.8	9.9	20.3	26.9	33.3			
	Moments (N*m)							
Muscle	Closed						Open	
L mAMES	3.09%	5.62%	4.41%	3.78%	4.51%		3.73%	5.89%
R mAMES	3.44%	5.55%	4.38%	4.09%	4.32%		4.18%	6.43%
L mAMEM	2.27%	1.69%	1.73%	0.91%	1.47%		3.07%	2.22%
R mAMEM	2.7%	1.67%	1.72%	0.98%	1.37%		3.14%	2.33%
L mAMEP	2.35%	1.54%	1.48%	1.27%	0.85%		2.83%	1.16%
R mAMEP	2.36%	1.48%	1.38%	1.22%	0.84%		2.83%	1.21%
L mAMP	10.3%	13.4%	14.3%	13.5%	12.4%		10.9%	13.1%
R mAMP	11.4%	12.2%	12.9%	12.9%	11.3%		12.1%	13.8%
L mPSTs	14.7%	11.5%	10.3%	8.90%	11.6%		17.5%	14.6%
R mPSTs	17.5%	12.0%	10.4%	9.23%	11.3%		16.8%	14.6%
L mPTd	15.0%	14.2%	17.7%	19.7%	16.4%		12.5%	8.02%
R mPTd	11.0%	13.1%	14.5%	18.4%	15.7%		6.96%	10.5%
L mPTv	2.13%	3.31%	2.40%	2.46%	3.88%		1.67%	2.62%
R mPTv	2.13%	2.73%	2.50%	2.68%	4.07%		1.80%	3.46%

Table 5. Summary of bite forces of *Alligator mississippiensis* calculated with 3D lever mechanics and FEA.

Bite Point	Specimen	Skull Length (cm)	Closed			Open		
			Lever Mechanics Bite Force (N)	FEA Bite Force (N)	Percent Difference	Lever Mechanics Bite Force (N)	FEA Bite Force (N)	Percent Difference
Posterior	AL 031	4.8	40.8	36.6	5.43%	33.5	37.0	4.63%
	AL 622	9.9	133	120	5.14%			
	AL 612	20.3	349	298	7.88%			
	AL 024	26.9	844	726	7.52%			
	AL 700	33.3	1170	1310	5.65%	984	1340	15.3%
Middle	AL 031	4.8	30.2	26.7	6.15%	27.5	26.3	2.23%
	AL 622	9.9	95.6	84.0	6.46%			
	AL 612	20.3	254	220	7.17%			
	AL 024	26.9	628	501	11.2%			
	AL 700	33.3	884	882	0.113%	676	901	14.3%
Anterior	AL 031	4.8	18.3	26.9	19.0%	13.5	27.0	33.3%
	AL 622	9.9	61.0	91.7	20.1%			
	AL 612	20.3	163	241	19.3%			
	AL 024	26.9	417	409	0.969%			
	AL 700	33.3	571	759	14.1%	426	736	26.7%

Table 6. Summary of jaw joint reaction forces of *Alligator mississippiensis* calculated with FEA.

Bite Point	Specimen	Skull Length (cm)	Closed		Open	
			Left Jaw Joint Force (N)	Right Jaw Joint Force (N)	Left Jaw Joint Force (N)	Right Jaw Joint Force (N)
Posterior	AL 031	4.8	39.7	40.4	40.0	40.0
	AL 622	9.9	131	141		
	AL 612	20.3	434	465		
	AL 024	26.9	843	879		
	AL 700	33.3	1490	1370	1480	1350
Middle	AL 031	4.8	337.0	38.7	36.7	38.3
	AL 622	9.9	144	140		
	AL 612	20.3	467	455		
	AL 024	26.9	885	881		
	AL 700	33.3	1640	1350	1620	1320
Anterior	AL 031	4.8	33.1	38.8	32.9	38.4
	AL 622	9.9	143	142		
	AL 612	20.3	435	454		
	AL 024	26.9	840	848		
	AL 700	33.3	1460	1340	1390	1300

Table 7. Summary of pterygomandibular joint (PMJ) reaction forces of *Alligator mississippiensis* for closed gape calculated with 3D lever mechanics.

Specimen	Skull Length (cm)		Left PMJ Force (N)	Right PMJ Force (N)
AL 031	4.8		19.1	12.8
AL 622	9.9		91.6	57.6
AL 612	20.3		128	105
AL 024	26.9		507	496
AL 700	33.3		995	896

Table 8. Components of bite force and joint reaction force of *Alligator mississippiensis* calculated with FEA for posterior bites.

Specimen	Reaction Point	Open				Closed			
		F _x (N)	F _y (N)	F _z (N)	F _{sum} (N)	F _x (N)	F _y (N)	F _z (N)	F _{sum} (N)
AL 031	Left Jaw Joint	30.4	25.5	1.00	39.7	31.1	23.3	9.28	40.0
	Right Jaw Joint	-34.8	-20.6	-0.116	40.4	-35.1	-18.2	-6.18	40.0
	Left Bite Point	2.46	-34.7	-11.4	36.6	0.595	-27.6	-24.6	37.0
AL 622	Left Jaw Joint	121	48.9	8.50	131				
	Right Jaw Joint	-120	-72.1	15.3	141				
	Left Bite Point	17.4	-117	-19.1	120				
AL 612	Left Jaw Joint	398	114	130	434				
	Right Jaw Joint	-415	-194	-79.7	465				
	Left Bite Point	39.5	-240	-173	298				
AL 024	Left Jaw Joint	701	295	314	823				
	Right Jaw Joint	-748	-460	-11.4	879				
	Left Bite Point	154	-681	-198	726				
AL 700	Left Jaw Joint	1280	767	42.1	1490	1260	699	349	1480
	Right Jaw Joint	-1290	-359	-169	1360	-1290	-268	-274	1350
	Left Bite Point	180	-1280	-58.4	1330	164	-1180	-618	1340

Table 9. Components of bite force and joint reaction force of *Alligator mississippiensis* calculated with FEA for intermediate bites.

Specimen	Reaction Point	Closed				Open			
		F _x (N)	F _y (N)	F _z (N)	F _{sum} (N)	F _x (N)	F _y (N)	F _z (N)	F _{sum} (N)
AL 031	Left Jaw Joint	33.9	13.8	-5.65	37.0	34.1	13.4	-1.96	36.7
	Right Jaw Joint	-32.7	-19.7	6.43	38.7	-32.5	-20.3	1.05	38.3
	Left Bite Point	-2.96	-24.0	-11.3	26.7	-5	-15.6	-20.6	26.3
AL 622	Left Jaw Joint	142	11.2	-22.9	144				
	Right Jaw Joint	-106	-73.7	55.5	140				
	Left Bite Point	-16.1	-78.0	-27.6	84.3				
AL 612	Left Jaw Joint	455	98.3	-42.9	467				
	Right Jaw Joint	-383	-242	40.5	455				
	Left Bite Point	-50.1	-178	-120	220				
AL 024	Left Jaw Joint	875	107	-77	885				
	Right Jaw Joint	-685	-471	293	881				
	Left Bite Point	-84.4	-482	-111	502				
AL 700	Left Jaw Joint	1550	413	-334	1640	1520	532	-157	1620
	Right Jaw Joint	-1150	-550	433	1350	-1120	-657	210	1320
	Left Bite Point	-252	-796	-285	882	-270	-619	-597	901

Table 10. Components of bite force and joint reaction force of *Alligator mississippiensis* calculated with FEA for anterior bites.

Specimen	Reaction Point	Closed				Open			
		F _x (N)	F _y (N)	F _z (N)	F _{sum} (N)	F _x (N)	F _y (N)	F _z (N)	F _{sum} (N)
AL 031	Left Jaw Joint	33.0	-1.48	1.70	33.1	32.8	-2.20	-0.885	32.9
	Right Jaw Joint	-34.6	-14.2	10.5	38.8	-34.2	-16.4	5.95	38.4
	Left Bite Point	-0.353	-14.2	-22.8	26.9	-1.99	-3.85	-26.6	27.0
AL 622	Left Jaw Joint	134	-34.7	34.5	143				
	Right Jaw Joint	-119	-60.0	49.6	142				
	Left Bite Point	4.11	-45.8	-79.3	91.7				
AL 612	Left Jaw Joint	423	-74.5	71.2	435				
	Right Jaw Joint	-409	-193	41.8	454				
	Left Bite Point	7.92	-52.5	-235	241				
AL 024	Left Jaw Joint	805	-161	177	840				
	Right Jaw Joint	-736	-375	193	848				
	Left Bite Point	36.7	-310	-265	409				
AL 700	Left Jaw Joint	1460	-98	25	1460	1390	-136	-33.0	1390
	Right Jaw Joint	-1200	-413	419	1340	-1200	-454	208	1300
	Left Bite Point	-63	-421	-629	759	-59.0	-154	-718	737

Table 11. Results of reduced major axis regression analyses for posterior bites at low gape. PMJ force has no specified bite point and is included here.

	Intercept	Slope	Lower Limit	Upper Limit	P Value	R²
Lever Mechanics Bite Force	0.4033	1.728	1.399	2.134	0.0006602	0.9866
FEA Bite Force	0.2940	1.790	1.349	2.374	0.001619	0.9757
Left Jaw Joint Force	0.3153	1.830	1.561	2.147	0.0002806	0.9924
Right Jaw Joint Force	0.3616	1.802	1.643	1.976	0.00005425	0.9975
Left PMJ Force	-0.09202	1.939	1.172	3.211	0.01020	0.9181
Right PMJ Force	-0.4320	2.138	1.347	3.394	0.007651	0.9322

Table 12. Results of reduced major axis regression analyses for intermediate bites at low gape.

	Intercept	Slope	Lower Limit	Upper Limit	P Value	R²
Lever Mechanics Bite Force	0.2556	1.740	1.390	2.179	0.0008008	0.9848
FEA Bite Force	0.1810	1.757	1.364	2.265	0.001161	0.9805
Left Jaw Joint Force	0.2592	1.897	1.646	2.187	0.0001992	0.9940
Right Jaw Joint Force	0.3391	1.815	1.655	1.989	0.00005316	0.9975

Table 13. Results of reduced major axis regression analyses for anterior bites at low gape.

	Intercept	Slope	Lower Limit	Upper Limit	P Value	R²
Lever Mechanics Bite Force	0.01742	1.777	1.422	2.221	0.0007795	0.9850
FEA Bite Force	0.2941	1.650	1.377	1.977	0.0004120	0.9902
Left Jaw Joint Force	0.2285	1.897	1.662	2.164	0.0001584	0.9948
Right Jaw Joint Force	0.3539	1.800	1.646	1.967	0.00004854	0.9976

LITERATURE CITED

- Bates KT and Falkingham PL. 2012. Estimating maximum bite performance in *Tyrannosaurus rex* using multi-body dynamics. *Biology Letters* 8: 660-664.
- Bramble DM. 1978. Origin of the Mammalian Feeding Complex: Models and Mechanisms. *Paleobiology* 4: 271-301.
- Busbey AB. 1989. Form and Function of the Feeding Apparatus of *Alligator mississippiensis*. *Journal of Morphology* 202: 99-127.
- Busbey AB. 1995. The structural consequences of skull flattening in crocodylians. In *Functional Morphology in Vertebrate Paleontology*, Thomason JJ (Ed.), Cambridge University Press, pp. 173-192.
- Carroll R. 1988. *Vertebrate Paleontology And Evolution*. W. H. Freeman and Company.
- Chatterjee S. 1985. *Postosuchus*, a New Thecodontian Reptile From the Triassic of Texas and the Origin of Tyrannosaurs. *Philosophical Transactions of the Royal Society of London* 309: 395-460.
- Cleuren J and De Vree F. 1992. Kinematics of the Jaw and Hyolingual Apparatus During Feeding in *Caiman crocodylus*. *Journal of Morphology* 212: 141-154.
- Cleuren J, Aerts P, and De Vree F. 1995. Bite and Joint Force Analysis in *Caiman crocodylus*. *Belgian Journal of Zoology* 12: 79-94.
- Curtis N, Jones MEH, Evans SE, O'Higgins P, and Fagan MJ. 2010. Feedback control from the jaw joints during biting: an investigation of the reptile *Sphenodon* using multibody modelling. *Journal of Biomechanics* 43: 3132-3137.
- Daniel WJT and McHenry C. 2001. Bite force to skull stress correlation— modelling the skull of *Alligator mississippiensis*. In *Crocodylian Biology And Evolution*, Grigg GC, Seebacher F, Franklin C. (Eds.), Surrey Beatty and Sons, Chipping Norton, NSW, pp. 135-143.
- Davis JL, Santana SE, Dumont ER, and Grosse IR. 2010. Predicting bite force in mammals: two-dimensional *versus* three-dimensional models. *Journal of Experimental Biology* 213: 1844-1851.
- Dumont ER and Herrel A. 2003. The effects of gape angle and bite point on bite force in bats. *Journal of Experimental Biology* 206: 2117-2123.

- Dumont ER. 2004. Patterns of diversity in cranial shape among plant-visiting bats. *Acta Chiropterologica* 6: 59-74.
- Erickson GM, Gignac PM, Lappin AK, Vliet KA, Brueggen JD, and Webb GJW. 2014. A comparative analysis of ontogenetic bite-force scaling among Crocodylia. *Journal of Zoology* 292: 48-55.
- Erickson GM, Gignac, PM, Stepan, SJ, Lappin, AK, Vliet, KA, Brueggen, JD, Inouye, BD, Kledzik, D, and Webb, GJW. 2012. Insights into the Ecology and Evolutionary Success of Crocodylians Revealed through Bite-Force and Tooth-Pressure Experimentation. *PLOS One*. 7:e31781.
- Erickson GM, Lappin AK, and Vliet KA. 2003. The ontogeny of bite-force performance in American alligator (*Alligator mississippiensis*). *Journal of the Zoological Society of London* 260: 317-327.
- Gignac PM and Erickson GM. 2015. Ontogenetic changes in dental form and tooth pressures facilitate developmental niche shifts in American alligators. *Journal of Zoology* 295: 132-142.
- Grosse IR, Dumont ER, Coletta C, and Tolleson A. 2007. Techniques for Modeling Muscle-Induced Forces in Finite Element Models of Skeletal Structures. *Anatomical Record* 290: 1069-1088.
- Herrel A, Podos J, Huber SK, and Hendry AP. 2005. Evolution of bite force in Darwin's finches: a key role for head width. *Journal of Evolutionary Biology* 18: 669-675.
- Herring SW and Herring SE. 1974. The Superficial Masseter and Gape in Mammals. *The American Naturalist*, 108: 561-5763.
- Holliday CM. 2009. New Insights Into Dinosaur Jaw Muscle Anatomy. *Anatomical Record* 292: 1246-1265.
- Holliday CM and Witmer LM. 2007. Archosaur Adductor Chamber Evolution: Integration of Musculoskeletal and Topological Criteria in Jaw Muscle Homology. *Journal of Morphology* 268: 457-484.
- Holliday CM, Tsai HP, Skijan RJ, George ID, and Pathan S. 2013. A 3D Interactive Model and Atlas of the Jaw Musculature of *Alligator mississippiensis*. *PLoS ONE* 8: e62806.

- Holliday CM, Sellers, KC, Vickaryous MK, Ross CF, Porro LB, Witmer LM, and Davis JL. The Functional and Evolutionary Significance of the Crocodyliform Pterygomandibular Joint. *Integrative and Comparative Biology* 54:1419.
- Iordankys NN. 1964. The jaw muscles of the crocodiles and some relating structures of the crocodilian skull. *Anatomischer Anzeiger* 115: 256-280.
- Iordankys NN. 2000. Jaw Muscles of the Crocodiles: Structures, Synonymy, and Some Implications of Homology and Functions. *Russian Journal of Herpetology* 7: 41-50.
- Langston W. 1973. The crocodilian skull in historical perspective. In *Biology of the Reptilia*, vol. 4, Gans C and Parsons TS (Eds.), London: Academic Press, pp. 263-289.
- McHenry CR, Clausen PD, Daniel WJT, Meers MB, and Pendharkar A. 2006. Biomechanics of the Rostrum in Crocodilians: A Comparative Analysis Using Finite-Element Modeling. *Anatomical Record Part A* 288: 827-849.
- Metzger KA, Daniel WJT, and Ross CF. 2005. Comparison of Beam Theory and Finite-Element Analysis With In Vivo Bone Strain Data From the Alligator Cranium. *Anatomical Record Part A* 283: 331-348.
- Metzger KA, Ross CF, and Spencer MA. 2003. Does the constrained lever model describe an optimality criterion in crocodilian jaw mechanics? *Integrative and Comparative Biology* 43: 825.
- Pfaller JB, Gignac PM, and Erickson GM. 2011. Ontogenetic changes in jaw-muscle architecture facilitate durophagy in the turtle *Sternotherus minor*. *Journal of Experimental Biology* 214: 1655-1667.
- Porro LB, Holliday CM, Anapol F, Ontiveros LC, Ontiveros LT, and Ross CF. 2011. *Journal of Morphology* 272: 910-937.
- Porro LB, Metzger KA, Iriarte-Diaz J, and Ross CF. 2013. *In vivo* bone strain and finite element modeling of the mandible of *Alligator mississippiensis*. *Journal of Anatomy* 223: 195-227.
- R Core Team. 2012. R: A language and environment for statistical computing. R Foundation for Statistical Computing, Vienna, Austria. ISBN 3-900051-07-0, URL <http://www.R-project.org/>

- Rayfield EJ and Milner AC. 2008. Establishing a framework for archosaur cranial mechanics. *Paleobiology* 34: 494-515.
- Rayfield EJ, Milner AC, Xuan VB, and Young PG. 2007. Functional Morphology of Spinosaur 'Crocodile-Mimic' Dinosaurs. *Journal of Vertebrate Paleontology* 27: 892-901.
- Sacks RD and Roy RR. 1982. Architecture of the hind limb muscles of cats: functional significance. *Journal of Morphology* 173: 185-195.
- Santana SE, Dumont ER, and Davis JL. 2010. Mechanics of bite force production and its relationship to diet in bats. *Functional Ecology* 24: 776-784.
- Santana SE, Geipel I, Dumont ER, Kalka MB, and Kalko EKV. 2011. All you can eat: High Performance Capacity and Plasticity in the Common Big-Eared Bat, *Micronycteris microtis* (Chiroptera: Phyllostomidae). *PLoS ONE* 6: e28584.
- Schumacher G-H. The Head Muscles and Hyolaryngeal Skeleton of Turtles and Crocodylians. In *Biology of the Reptilia*, vol. 4, Gans C and Parsons TS (Eds.), London: Academic Press, pp. 101-199.
- Schwimmer DR. 2002. King of the Crocodylians: The Paleobiology of *Deinosuchus*. Indiana University Press.
- Sinclair AG and Alexander RM. 1987. Estimates of forces exerted by the jaw muscles of some reptiles. *Journal of the Zoological Society of London* 2013: 107-115.
- Slater GJ, Dumon ER, and Van Valkenburgh B. 2009. Implications of predatory specialization for cranial form and function in canids. *Journal of Zoology* 278: 181-188.
- Strait DS, Wang Q, Dechow PC, Ross CF, Richmond BG, Spencer MA, and Patel BA. 2005. Modeling elastic properties in finite element analysis: how much precision is needed to produce an accurate model? *Anatomical Record A* 283A: 275-287.
- Walker AD. 1990. A Revision of *Sphenosuchus acutus* Haughton, a Crocodylomorph Reptile from the Elliot Formation (Late Triassic or Early Jurassic) of South Africa. *Philosophical Transactions: Biological Sciences* 330: 1-120.